Rationally designed hierarchical N-doped carbon@NiCo2O4 double-shelled nanoboxes for enhanced visible light CO2 reduction

Wang, Sibo; Guan, Bu Yuan; Lou, David Xiong Wen

2018

Wang, S., Guan, B. Y., & Lou, D. X. W. (2018). Rationally designed hierarchical N-doped carbon@NiCo2O4 double-shelled nanoboxes for enhanced visible light CO2 reduction. Energy & Environmental Science, 11, 306-310. doi:10.1039/c7ee02934a

https://hdl.handle.net/10356/138610

https://doi.org/10.1039/C7EE02934A

Journal Name

COMMUNICATION

Rationally designed hierarchical N-doped carbon@$NiCo_2O_4$ double-shelled nanoboxes for enhanced visible light CO_2 reduction

Sibo Wang, Bu Yuan Guan and Xiong Wen (David) Lou*

Received 00th January 20xx,
Accepted 00th January 20xx

DOI: 10.1039/x0xx00000x

www.rsc.org/

Here we demonstrate the delicate design and construction of hierarchical nitrogen-doped carbon@$NiCo_2O_4$ (NC@$NiCo_2O_4$) double-shelled nanoboxes for photocatalytic reduction of CO_2 with visible light. This smart design rationally combines the structural and functional advantages of catalytically active Co and Ni species with conductive nitrogen-doped carbon into a three-dimensional hollow nanoarchitecture, which can remarkably facilitate the migration and separation of photogenerated charge carriers, enhance the adsorption and concentration of CO_2 molecules, and provide more active sites for photochemical reactions. Benefitting from these unique structural and compositional features, the hierarchical NC@$NiCo_2O_4$ double-shelled nanoboxes manifest considerable performance for deoxygenative reduction of CO_2 with high CO-evolving rate (26.2 μmol h^{-1}; 2.62×10^4 μmol h^{-1} g^{-1}) and high stability.

Reduction of carbon dioxide (CO_2) with abundant solar energy to generate valuable energetic molecules (e.g., CO, CH_4, HCOOH and CH_3OH) has long been an ideal solution to explore renewable energy and relieve global warming.[1-5] However, the efficient photocatalytic CO_2 reduction by artificial materials is very challenging, mainly due to the high thermodynamic stability of linear CO_2 molecules and high recombination rate of charge carriers during photocatalysis.[4] Therefore, the construction of CO_2 photoreduction systems typically necessitates the synergetic operation of photosensitizers,[7-10] CO_2 absorbers/activators[11-16] and electron mediators[17-22] in a harmonious manner. Transition metal ions with multiple redox states are favorable components to build electron transport chains for CO_2 conversion, which can effectively prevent the formation of unwanted high-energy intermediates and thus promote the multi-electron reduction of CO_2, particularly when the process is combined with protons.[11,18,20] Cobalt and nickel oxides/complexes have been demonstrated as efficient catalysts to accelerate charge migration kinetics, CO_2 activation and surface reaction in photochemical CO_2 reduction.[8,11,14,16,18,21]

Mixed metal oxides with two-dimensional (2D) architectures have sparked growing interests in diverse areas owing to their ample redox functions, high chemical stabilities, and abundant optical and electronic characteristics.[23-27] Of note, the configuration of 2D nanosheets can effectively reduce the diffusion length of charge carriers, provide high surface area and expose rich catalytically active sites, which are highly desirable to promote photoredox reactions.[23,25,28] On the other hand, compositing semiconductors with carbonaceous materials is an effective strategy to enhance photocatalytic activity because of their outstanding light harvesting and anti-photocorrosion properties.[29-31] Importantly, the electron-accepting/-transfer features of the introduced carbon species can render a convenient path to direct the flow of charge carriers, prolonging their lifetime and eventually leading to enhanced photocatalytic performance. Meanwhile, it is considered that nitrogen-doping can further ameliorate the electronic and chemical functions of carbon-based materials and thus enhance the photo(electro)chemical performances.[32-34] In addition, the achievement of efficient photocatalysis also depends on delicate design and construction of catalysts with proper structures.

Hollow structured materials with various architectures and tailored compositions have shown advantages in widespread applications in energy storage and conversion areas.[35-37] Recently, hollow micro/nanostructures have been introduced to photoredox catalytic field as powerful light transducers to upgrade the performance.[38-45] In regard of CO_2 photoreduction, hollow nanostructures hold several inherent advantages over the solid counterparties. Specifically, the interior cavity not only favors the separation of photogenerated electron-hole pairs by

School of Chemical and Biomedical Engineering, Nanyang Technological University, 62 Nanyang Drive, Singapore, 637459, Singapore
E-mail: xwlou@ntu.edu.sg; davidlou88@gmail.com
Webpage:http://www.ntu.edu.sg/home/xwlou/

† Electronic Supplementary Information (ESI) available: Detailed experimental procedures, additional FESEM images, TEM images, XRD patterns, EDX spectrum, XPS spectra, DRS, Nyquist plots, PL spectra, and detailed photocatalytic CO_2 reduction reactions. See DOI: 10.1039/x0xx00000x

reducing diffusion distance from bulk to surface, but also provides large surface area to promote CO_2 adsorption and surface-dependant redox reactions on both the exterior and interior shells.[38,40,43,45] Besides, the permeable shells can be deliberately decorated or engineered with cocatalysts or other functional materials to accelerate charge mobility kinetics and CO_2 activation at their interfaces.[12,38,40,42] Moreover, photo adsorption could be enhanced by multi-light scattering/reflection in the hollow cavities,[40] especially in nanoboxes.[41] Indeed, several seminal works have demonstrated the prodigious opportunities for CO_2 photoreduction by hollow structured materials, such as CuO-$TiO_{2-x}N_x$ hollow nanocubes,[38] $Ti_{0.91}O_2$@graphene hollow spheres,[43] and Bi_2WO_6 hollow microspheres.[45] Despite these achievements, it remains a significant challenge to design and construct well-defined hierarchical hollow architectures to integrate these structural and compositional merits mentioned above and fully realize their advantages for photocatalytic CO_2 reduction.

Herein, we demonstrate the design and synthesis of hierarchical hollow nanostructures composed of ultrathin $NiCo_2O_4$ nanosheets and nitrogen-doped carbon nanoboxes for deoxygenative reduction of CO_2 with visible light. The overall synthetic strategy involves several steps, as schematically illustrated in Fig. 1. Starting with Fe_2O_3 nanocube as the template, a thin layer of polydopamine (PDA) is coated on the Fe_2O_3 particle through the sol-gel method (step I). Then, the Fe_2O_3@PDA core-shelled nanocube is heated under N_2 atmosphere to transform the PDA layer to N-doped carbon (NC) shell. Next, the oxide core is dissolved selectively by acid etching, generating a NC nanobox (step II). Finally, a layer of ultrathin $NiCo_2O_4$ nanosheets is grown on the NC nanobox *via* a facile hydrothermal reaction followed by a thermal treatment, producing the hierarchical NC@$NiCo_2O_4$ double-shelled nanobox (step III). These hierarchical nanoboxes synergistically combine the structural and functional advantages of both Ni-Co based catalytically active species and carbon-based electron-accepting/-transfer support, which is a perfect nanosystem to study the relationship between structure/composition and CO_2 photoconversion performance. Impressively, when cooperated with a visible light photosensitizer under mild conditions, the NC@$NiCo_2O_4$ nanoboxes exhibit considerable activity (26.2 μmol h^{-1}; 2.62×10^4 μmol h^{-1} g^{-1}) and high stability for selectively reducing CO_2 into CO.

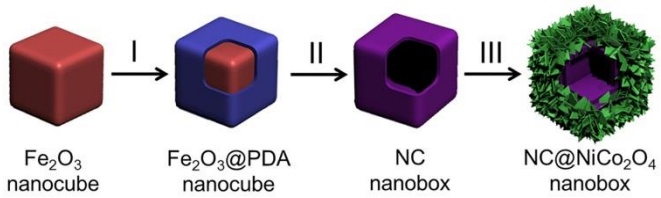

Fig. 1 Schematic illustration of the synthetic process of hierarchical NC@$NiCo_2O_4$ double-shelled nanoboxes. (I) PDA coating, (II) annealing under N_2 atmosphere and acid etching, (III) growth of $NiCo_2O_4$ nanosheets.

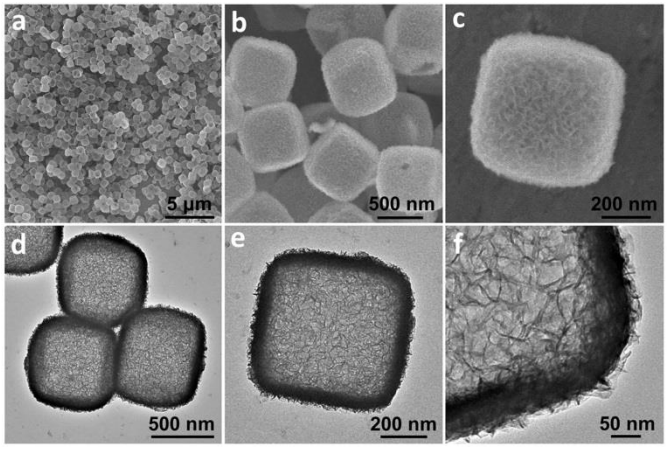

Fig. 2 (a-c) FESEM and (d-f) TEM images of hierarchical NC@Ni-Co LDH double-shelled nanoboxes.

Highly uniform Fe_2O_3 nanocubes with an average size of *ca.* 500 nm are prepared as the template through a hydrothermal method (Fig. S1 and Fig. S2, ESI†).[46] Then, the Fe_2O_3 nanocubes are further coated with a layer of PDA. Uniform Fe_2O_3@PDA core-shelled nanocubes with the particle size of *ca.* 580 nm are obtained (Fig. S3, ESI†). After a carbonization process under N_2 atmosphere at 500 °C for 3 h, the PDA layer is converted into the NC shell while the Fe_2O_3 core is reduced to Fe_3O_4 cube, leading to the formation of Fe_3O_4@NC core-shelled nanocubes (Fig. S4 and Fig. S5, ESI†). The as-derived Fe_3O_4@NC core-shelled nanocubes are etched by 4 M HCl at 70 °C for 1 h to completely remove the Fe_3O_4 cores, generating uniform NC nanoboxes with smooth surface and shell thickness of *ca.* 30 nm (Fig. S6, ESI†). The obtained NC nanoboxes are then modified with polyvinylpyrrolidone (PVP) and dispersed in a H_2O/ethanol mixture to grow a layer of Ni-Co layered double hydroxide (LDH) nanosheets.[47] Field-emission scanning electron microscopy (FESEM) images show that a layer of Ni-Co LDH nanosheets is uniformly grown on the NC nanoboxes (abbreviated as NC@Ni-Co LDH) (Fig. 2a-c). A closer examination on the shell of a NC@Ni-Co LDH nanobox reveals the layer is composed of randomly assembled ultrathin nanosheets (Fig. 2c). Transmission electron microscopy (TEM) images demonstrate the hollow feature of NC@Ni-Co LDH nanoboxes (Fig. 2d,e). As revealed in the magnified TEM image, the hierarchical layer of a Ni-Co LDH nanosheets with the thickness of *ca.* 75 nm can be clearly discerned (Fig. 2f). No noticeable interlayer gap can be observed between the NC shell and the Ni-Co LDH layer, suggesting the Ni-Co LDH nanosheets are tightly coupled on the NC nanoboxes. This architecture ensures the strong interaction between NC nanobox and $NiCo_2O_4$ nanosheets in the final NC@$NiCo_2O_4$ product, which guarantees efficient charge transportation for redox reactions. Irregular bulk particles composed of Ni-Co LDH nanosheets are prepared as a control sample under the same conditions without NC nanoboxes as the templates (Fig. S7, ESI†).

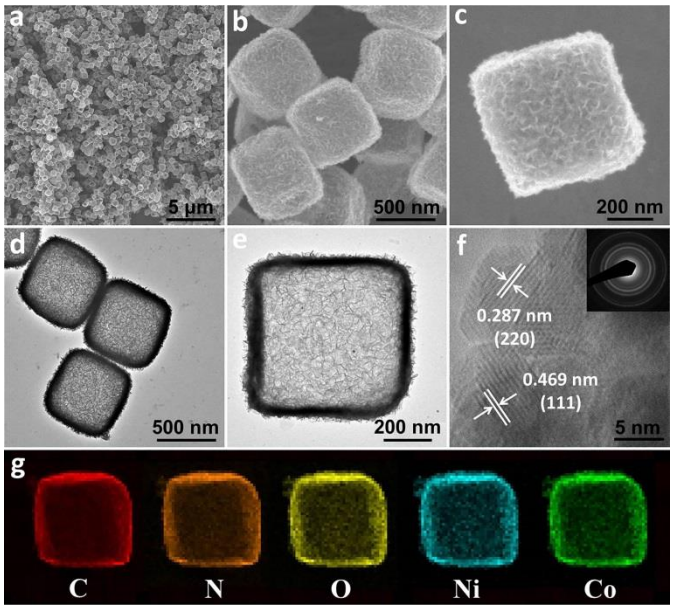

Fig. 3 (a-c) FESEM and (d,e) TEM images of hierarchical NC@$NiCo_2O_4$ double-shelled nanoboxes, (f) HRTEM image of the $NiCo_2O_4$ nanosheets and SAED pattern (inset) of NC@$NiCo_2O_4$ nanoboxes , and (g) EDX mappings of an individual NC@$NiCo_2O_4$ nanobox.

The as-prepared NC@Ni-Co LDH nanoboxes can withstand the annealing treatment in air at 300 °C. EDX analysis of the pyrolysis product shows the existence of Co, Ni, C, N, and O elements in the sample (Fig. S8, ESI†). The percentage of NC remained in the final hybrid product is *ca.* 8.13 wt.%. These highly conductive NC layers would promote electron transfer during photocatalysis. The valence states of Co and Ni in the NC@$NiCo_2O_4$ nanoboxes are identified by X-ray photoelectron spectroscopy (XPS) measurements (Fig. S9, ESI†). The results indicate the co-existence of two solid redox couples (Ni^{2+}/Ni^{3+} and Co^{2+}/Co^{3+}) in the catalysts,[21] which could provide abundant active sites for heterogeneous CO_2 photoreduction. The XRD pattern (Fig. S10, ESI†) of the product can be indexed to spinel $NiCo_2O_4$ phase (JCPDS card No. 20-0781). No residues or impurity phases are detected, indicating the NC@Ni-Co LDH precursors are completely converted to NC@$NiCo_2O_4$ nanoboxes after the thermal treatment. The $NiCo_2O_4$ species with high crystallinity in NC@$NiCo_2O_4$ product are also favorable for facilitating electron mobility in photoredox reactions. FESEM images of the as-obtained NC@$NiCo_2O_4$ nanoboxes reveal the cubic morphology and the ultrathin sheet-shaped subunits (Fig. 3a-c) TEM images validate the hierarchical hollow nanostructure of the NC@$NiCo_2O_4$ particles (Fig. 3d,e). High-resolution TEM (HRTEM) image shows the edge view of the $NiCo_2O_4$ nanosheets with clear lattice fringes (Fig. 3f). The interlayer distances are calculated to be *ca.* 0.287 and 0.469 nm, corresponding to the (220) and (111) crystal planes of spinel $NiCo_2O_4$ phase, respectively. The polycrystalline nature of the $NiCo_2O_4$ nanosheets is confirmed by the selected area electron diffraction (SAED) pattern (insert, Fig. 3f), which can be indexed to the spinel $NiCo_2O_4$ phase as well. Elemental mappings are performed to examine the inhomogeneous distribution of NC and $NiCo_2O_4$ in the NC@$NiCo_2O_4$ double-shelled nanobox. The results show that the intensities of N and C elements are slightly stronger in the inner edge of the shell, which is different from that of Ni, Co, and O elements (Fig. 3g). N_2 sorption measurements reveal the hierarchical NC@$NiCo_2O_4$ nanoboxes possess a high Brunauer-Emmett-Teller (BET) surface area of 142 $m^2\ g^{-1}$ (Fig. S11, ESI†), which is about twice that of the nanosheet-assembled $NiCo_2O_4$ solids (67 $m^2\ g^{-1}$). The benefit of such high surface area for improving CO_2 adsorption/concentration is demonstrated by CO_2 adsorption measurements. As shown in Fig. 4a, the NC@$NiCo_2O_4$ nanoboxes exhibit a maximum CO_2 uptake of *ca.* 60 $cm^3\ g^{-1}$ at 0 °C under 1 atm, much higher than that of bulk $NiCo_2O_4$ particles. The CO_2 adsorption results indicate the hierarchical NC@$NiCo_2O_4$ double-shelled nanoboxes show a pronounced advantage in CO_2 adsorption/concentration, suggesting their great potential for CO_2 conversion catalysis.

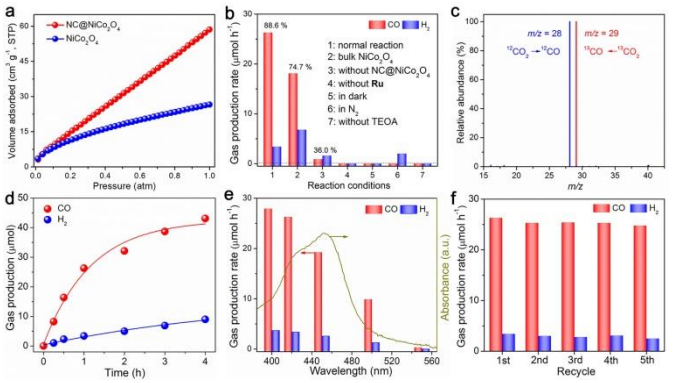

Fig. 4 (a) CO_2 adsorption isotherms of NC@$NiCo_2O_4$ nanoboxes and bulk $NiCo_2O_4$ particles at 0 °C. (b) Production of CO and H_2 from photocatalytic CO_2 reduction system under various reaction conditions. The inserted percentage indicates the selectivity of CO. (c) Results of GC-MS analysis for produced CO using $^{13}CO_2$ and $^{12}CO_2$ as gas sources, respectively. (d) Evolution of CO and H_2 as a function of reaction time. (e) Wavelength dependence of yield of CO and H_2, and the light absorption spectrum of the **Ru** photosensitizer. The wavelength of incident light is controlled by applying appropriate long-pass cut-off filters. (f) Generation of CO and H_2 in stability tests.

Catalytic performances of the hierarchical NC@$NiCo_2O_4$ double-shelled nanoboxes were evaluated by visible light driven CO_2 photoreduction reactions conducted in H_2O/acetonitrile mixture under mild reaction conditions (30 °C, 1 atm CO_2) with $[Ru(bpy)_3]Cl_2{\cdot}6H_2O$ (abbreviated as **Ru**, bpy = 2'2-bipyridine) and triethanolamine (TEOA) as the photosensitizer and electron donor, respectively. Fig. 4b shows the performance of the CO_2 reduction catalysis under various reaction conditions. In the normal reaction (column 1, Fig. 4b), a large amount of CO (26.2 μmol h^{-1}; 2.62×10^4 μmol $h^{-1}\ g^{-1}$) and a small production of H_2 (3.4 μmol h^{-1}) are generated from the reaction system, corresponding to a high CO selectivity of 88.6 %. The CO_2 photoreduction system manifests a high apparent quantum yield (AQY) of 1.07 % under monochromatic light irradiation of 420 nm. The achieved CO_2 reduction rate is superior to many other systems (Table S1, ESI†).[3,7-15,17,19,21,48-52] When the CO_2 photoreduction reaction was conducted with bulk $NiCo_2O_4$ as the catalyst, the yield (18.3 μmol h^{-1}) and selectivity (74.7 %) of CO product obviously reduced (column 2, Fig. 4b). Furthermore, if the NC@$NiCo_2O_4$ catalyst was not added into the reaction system, the evolution of CO (0.9 μmol h^{-1}) together with CO

selectivity (36 %) decreased significantly (column 3, Fig. 4b). These results indicate that this tandem catalytic system is mainly responsible for the CO_2-to-CO transformation reaction with considerable efficiency. The hierarchical NC@$NiCo_2O_4$ nanoboxes are capable of enhancing the adsorption/concentration of CO_2 molecules and accelerating the transport kinetics of photo-triggered charges. No hydrocarbon products are detected from the developed system, consistent with the results of reported works.[11,14,20] The CO_2 reduction reaction is completely terminated without the presence of **Ru** or visible light irradiation (column 4 and column 5, Fig. 4b), indicating the reaction is started by photocatalysis. When using N_2 to replace CO_2 to perform the reaction under identical conditions (column 6, Fig. 4b), the system only produces a small amount of H_2, no evolution of CO can be detected. This observation suggests the generated CO is originated from the CO_2 reactant. The control experiment without TEOA indicates that no detectable CO is produced, revealing that the sacrificial agent greatly affects the performance of the catalyst.[11,14,15,49,50]

To provide solid proof for the carbon source of CO, ^{13}C-labelled isotropic experiments are conducted and the produced gases are analysed by gas chromatography-mass spectrometer (GC-MS). Only ^{13}CO (*m/z* = 29) can be detected when $^{13}CO_2$ is employed as the gas source (Fig. 4c). The above findings show that the CO is generated from photosplitting of CO_2 molecules. The time course for the yields of CO and H_2 is depicted in Fig. 4d. The accumulated product is *ca.* 52 μmol for the 4 h reaction, affording a catalytic turnover number (TON) of *ca.* 14 with respect to $NiCo_2O_4$ in the hybrid catalyst. This TON value is comparable to other reported works.[8,48,53] The decrease in CO_2-to-CO conversion rate after long-time reaction is mainly attributed to photobleaching of the dye photosensitizer.[11,14,16,49,50] The catalytic activities of the NC@$NiCo_2O_4$ nanoboxes for CO_2 photoreduction are further studied under different wavelength illumination. As shown in Fig. 4e, the variation tendency of gas evolution is matched well with the optical absorption spectrum of the **Ru** complex, rather than that of the NC@$NiCo_2O_4$ material (Fig. S12, ESI†). This observation indicates the CO_2 reduction reaction is driven photocatalytically by the harvested light photons of **Ru** photosensitizer.[11] Stability of the NC@$NiCo_2O_4$ catalyst is then evaluated. As presented in Fig. 4f, the gas formation in each consecutive cycle is almost unchanged, demonstrating the high stability of the NC@$NiCo_2O_4$ catalyst.

Photoelectrochemical characterizations are carried out to demonstrate the crucial role of hierarchical NC@$NiCo_2O_4$ nanoboxes for promoting transfer kinetics of charge carriers during CO_2 photoreduction. Benefitting from the high electric conductivity of NC inner layers, NC@$NiCo_2O_4$ catalysts exhibit much lower electronic resistance than solid $NiCo_2O_4$ sample (Fig. S13, ESI†). The increased electronic conductivity is effective for accelerating the migration of charge carriers. On the other hand, the separation-recombination rate of photo-excited charges of the CO_2 reduction system is investigated by in situ room temperature photoluminescence (PL) measurements under excitation wavelength of 500 nm (Fig. S14, ESI†). The PL intensity of the CO_2 reduction system is remarkably diminished in the presence of NC@$NiCo_2O_4$ catalyst. The PL quenching principally reflects an inhibited recombination rate of charge carriers, which can greatly augment heterogeneous CO_2 conversion. These photoelectrochemical observations evidence the function of NC@$NiCo_2O_4$ nanoboxes for boosting the separation and transport of photogenerated charge carriers in the CO_2 reduction system, and thereby markedly improving the catalytic performance.

Conclusions

In summary, hierarchical NC@$NiCo_2O_4$ double-shelled nanoboxes are rationally prepared as a highly efficient catalyst for visible light CO_2 reduction. These hybrid hollow structures hold unique structural and compositional features with reduced diffusion length and improved electronic conductivity for separation and transport of charge carriers, large surface area for CO_2 adsorption/concentration, and more active sites for photoredox catalysis. Consequently, the NC@$NiCo_2O_4$ catalyst exhibits remarkable photocatalytic performance for deoxygenative reduction of CO_2 with high CO evolution rate (26.2 μmol h^{-1}; 2.62×10^4 μmol h^{-1} g^{-1}) and good stability. All these findings demonstrate rational design and synthesis of hierarchical hollow nanostructures can be an efficient strategy to achieve highly active materials for CO_2 photoreduction. This work might encourage the study on hollow photosynthetic nanostructures for solar energy-related applications.

Acknowledgements

X. W. Lou acknowledges the funding support from the National Research Foundation (NRF) of Singapore via the NRF investigatorship (NRF-NRFI2016-04).

Notes and references

1 A. Listorti, J. Durrant and J. Barber, *Nat. Mater.*, 2009, **8**, 929.
2 N. S. Lewis and D. G. Nocera, *Proc. Natl. Acad. Sci. USA*, 2006, **103**, 15729.
3 R. Kuriki, M. Yamamoto, K. Higuchi, Y. Yamamoto, M. Akatsuka, D. Lu, S. Yagi, T. Yoshida, O. Ishitani and K. Maeda, *Angew. Chem. Int. Ed.*, 2017, **56**, 4867.
4 J. Tang, J. R. Durrant and D. R. Klug, *J. Am. Chem. Soc.*, 2008, **130**, 13885.
5 K. Li, A. D. Handoko, M. Khraisheh and J. Tang, *Nanoscale*, 2014, **6**, 9767.
6 T. Sakakura, J. C. Choi and H. Yasuda, *Chem. Rev.*, 2007, **107**, 2365.
7 R. Kuriki, H. Matsunaga, T. Nakashima, K. Wada, A. Yamakata, O. Ishitani and K. Maeda, *J. Am. Chem. Soc.*, 2016, **138**, 5159.
8 C. Gao, Q. Meng, K. Zhao, H. Yin, D. Wang, J. Guo, S. Zhao, L. Chang, M. He, Q. Li, H. Zhao, X. Huang, Y. Guo and Z. Tang, *Adv. Mater.*, 2016, **28**, 6485.
9 H. Zhang, J. Wei, J. Dong, G. Liu, L. Shi, P. An, G. Zhao, J. Kong, X. Wang, X. Meng, J. Zhang and J. Ye, *Angew. Chem. Int. Ed.*, 2016, **55**, 14310.
10 L. Shi, T. Wang, H. Zhang, K. Chang and J. Ye, *Adv. Funct. Mater.*, 2015, **25**, 5360.
11 S. Wang, W. Yao, J. Lin, Z. Ding and X. Wang, *Angew. Chem. Int. Ed.*, 2014, **53**, 1034.

12 W. Tu, Y. Zhou and Z. Zou, *Adv. Mater.*, 2014, **26**, 4607.
13 T. Kajiwara, M. Fujii, M. Tsujimoto, K. Kobayashi, M. Higuchi, K. Tanaka and S. Kitagawa, *Angew. Chem. Int. Ed.*, 2016, **55**, 2697.
14 T. Ouyang, H. H. Huang, J. W. Wang, D. C. Zhong and T. B. Lu, *Angew. Chem. Int. Ed.*, 2017, **56**, 738.
15 H. Q. Xu, J. Hu, D. Wang, Z. Li, Q. Zhang, Y. Luo, S. H. Yu and H. L. Jiang, *J. Am. Chem. Soc.*, 2015, **137**, 13440.
16 V. S. Thoi, N. Kornienko, C. G. Margarit, P. Yang and C. J. Chang, *J. Am. Chem. Soc.*, 2013, **135**, 14413.
17 S. Sato, T. Morikawa, S. Saeki, T. Kajino and T. Motohiro, *Angew. Chem. Int. Ed.*, 2010, **49**, 5101.
18 H. Takeda and O. Ishitani, *Coordin. Chem. Rev.*, 2010, **254**, 346.
19 Y. Fu, D. Sun, Y. Chen, R. Huang, Z. Ding, X. Fu and Z. Li, *Angew. Chem. Int. Ed.*, 2012, **51**, 3364.
20 J. M. Lehn and R. Ziessel, *Proc. Nat. Acad. Sci. USA*, 1982, **79**, 701.
21 Z. Wang, M. Jiang, J. Qin, H. Zhou and Z. Ding, *Phys. Chem. Chem. Phys.*, 2015, **17**, 16040.
22 B. Cui, H. Lin, Y. Z. Liu, J. B. Li, P. Sun, X. C. Zhao and C. J. Liu, *J Phys. Chem. C*, 2009, **113**, 14083.
23 Y. Zhou, Y. Zhang, M. Lin, J. Long, Z. Zhang, H. Lin, J. C. S. Wu and X. Wang, *Nat. Commun.*, 2015, **6**, 8340.
24 J. L. Gunjakar, T. W. Kim, H. N. Kim, I. Y. Kim and S. J. Hwang, *J. Am. Chem. Soc.*, 2011, **133**, 14998.
25 S. Liang, L. Wen, S. Lin, J. Bi, P. Feng, X. Fu and L. Wu, *Angew. Chem. Int. Ed.*, 2014, **53**, 2951.
26 K. Teramura, S. Iguchi, Y. Mizuno, T. Shishido and T. Tanaka, *Angew. Chem. Int. Ed.*, 2012, **51**, 8008.
27 C. Yuan, H. B. Wu, Y. Xie and X. W. Lou, *Angew. Chem. Int. Ed.*, 2014, **53**, 1488.
28 J. Zhang, Y. Chen and X. Wang, *Energy Environ. Sci.*, 2015, **8**, 3092.
29 Q. Wang, T. Hisatomi, Y. Suzuki, Z. Pan, J. Seo, M. Katayama, T. Minegishi, H. Nishiyama, T. Takata, K. Seki, A. Kudo, T. Yamada and K. Domen, *J. Am. Chem. Soc.*, 2017, **139**, 1675.
30 Y. X. Pan, Y. You, S. Xin, Y. Li, G. Fu, Z. Cui, Y. L. Men, F. F. Cao, S. H. Yu and J. B. Goodenough, *J. Am. Chem. Soc.*, 2017, **139**, 4123.
31 Y. J. Xu, Y. Zhuang and X. Fu, *J. Phys. Chem. C*, 2010, **114**, 2669.
32 S. Liu, J. Tian, L. Wang, Y. Zhang, X. Qin, Y. Luo, A. M. Asiri, A. O. Al-Youbi and X. Sun, *Adv. Mater.*, 2012, **24**, 2037.
33 X. Yang, C. Cao, L. Erickson, K. Hohn, R. Maghirang and K. Klabunde, *J. Catal.*, 2008, **260**, 128.
34 S. Peng, L. Li, S. G. Mhaisalkar, M. Srinivasan, S. Ramakrishna and Q. Yan, *ChemSusChem*, 2014, **7**, 2212.
35 L. Yu, H. B. Wu and X. W. Lou, *Acc. Chem. Res.*, 2017, **50**, 293.
36 B. Y. Guan, L. Yu, J. Li and X. W. Lou, *Sci. Adv.*, 2016, **2**, e1501554.
37 S. Wang, B. Y. Guan, L. Yu and X. W. Lou, *Adv. Mater.*, 2017, **29**, 1702724.
38 S. I. In, D. D. Vaughn and R. E. Schaak, *Angew. Chem. Int. Ed.*, 2012, **51**, 3915.
39 T. Zhu, H. B. Wu, Y. Wang, R. Xu and X. W. Lou, *Adv. Energy Mater.*, 2012, **2**, 1497.
40 J. Sun, J. Zhang, M. Zhang, M. Antonietti, X. Fu and X. Wang, *Nat. Commun.*, 2012, **3**, 1139.
41 B. Qiu, Q. Zhu, M. Du, L. Fan, M. Xing and J. Zhang, *Angew. Chem. Int. Ed.*, 2017, **56**, 2684.
42 D. Zheng, X. N. Cao and X. Wang, *Angew. Chem. Int. Ed.*, 2016, **55**, 11512.
43 W. Tu, Y. Zhou, Q. Liu, Z. Tian, J. Gao, X. Chen, H. Zhang, J. Liu and Z. Zou, *Adv. Funct. Mater.*, 2012, **22**, 1215.
44 S. Wang, B. Y. Guan, Y. Lu and X. W. Lou, *J. Am. Chem.Soc.*, 2017, **139**, 17305.
45 H. Cheng, B. Huang, Y. Liu, Z. Wang, X. Qin, X. Zhang and Y. Dai, *Chem. Commun.*, 2012, **48**, 9729.
46 X. Y. Yu, H. Hu, Y. Wang, H. Chen and X. W. Lou, *Angew. Chem. Int. Ed.*, 2015, **54**, 7395.
47 L. Huang, D. Chen, Y. Ding, S. Feng, Z. L. Wang and M. Liu, *Nano Lett.*, 2013, **13**, 3135.
48 K. Niu, Y. Xu, H. Wang, R. Ye, H. L. Xin, F. Lin, C. Tian, Y. Lum, K. C. Bustillo, M. M. Doeff, M. T. M. Koper, J. Ager, R. Xu and H. Zheng, *Sci. Adv.*, 2017, **3**, e1700921.
49 Y. Wang, N. Y. Huang, J. Q. Shen, P. Q. Liao, X. M. Chen and J. P. Zhang, *J. Am. Chem. Soc.*, 2018, DOI: 10.1021/jacs.7b10107
50 X. Lin, Y.Gao, M. Jiang, Y. Zhang, Y. Hou, W. Dai, S. Wang and Z. Ding, *Appl. Catal. B Environ.*, 2018, **224**, 1009.
51 C. Huang, C. Chen, M. Zhang, L. Lin, X. Ye, S. Lin, M. Antonietti and X. Wang, *Nat. Commun.*, 2015, **6**, 7698.
52 Y. Zheng, L. Lin, X. Ye, F. Guo and X. Wang, *Angew. Chem. Int. Ed.*, 2014, **53**, 11926.
53 G. A. Andrade, A. J. Pistner, G. P. Yap, D. A. Lutterman and J. Rosenthal, *ACS Catal.*, 2013, **3**, 1685.